Recent Advances in Ball-Milling-Based Silicon Anodes for Lithium-Ion Batteries

Han Yang [1,†]**, Shiyu Lin** [1,†]**, Alex Cheng** [2]**, Fangbo He** [3]**, Zhoulu Wang** [1]**, Yutong Wu** [1]**, Yi Zhang** [1,*] **and Xiang Liu** [1,*]

1 School of Energy Sciences and Engineering, Nanjing Tech University, Nanjing 211816, China
2 Shanghai Energy New Materials Technology Co., Ltd., Shanghai 201399, China
3 Zhuhai Energy New Materials Technology Co., Ltd., Zhuhai 519600, China
* Correspondence: zhangy@njtech.edu.cn (Y.Z.); iamxliu@njtech.edu.cn (X.L.)
† These authors contributed equally to this work.

Abstract: Having a high theoretical capacity density of 4200 mAh g^{-1}, silicon has been highlighted as one of the most promising anode materials for lithium-ion batteries. Countless silicon-based materials have been proposed and reported in research articles, mostly synthesized using bottom-up methods. While the infamous volume expansion issue can be settled with the bottom-up processes, the complicated protocols and high cost leave a non-neglectable gap between laboratory-scale and mass production. The top-down ball-milling method is still favored by industrial suppliers because of its simplicity and cost-effectiveness, even with compromised electrochemical performances. This paper reviews the latest development of ball-milling-based silicon anode materials. Although the ball-milling process seems straightforward, the procedures and parameters influencing the product have hardly been discussed in research papers compared to the bottom-up ones. This paper reviews recent advances in ball-milling-based silicon anode materials, provides a material comparison, and discusses how ball milling can provide lithium-ion batteries with greater possibilities at a larger scale.

Keywords: ball mill; Si anode; lithium-ion battery; electric vehicle; electrochemistry

1. Introduction

In the early times of energy storage research, secondary batteries represented by nickel metal hydride and lead acid systems were widely applied [1,2]. However, their energy density (<100 Wh/kg) [3] cannot fully meet the increasing demand, limiting subsequent development. Having a small radius of ions, high carrier diffusion coefficient, low density, and high specific capacity [4], lithium metal soon became an important candidate in battery research. With the continuous understanding of organic electrolytes and layered compounds [5], lithium metal secondary batteries have developed rapidly, but the lithium dendrite problem forced the [6] research on the battery to stagnate [7]. After the Nobel-price-winning rocking-chair lithium-ion batteries (LIBs) were developed and commercialized in the 1980–90s, lithium-based batteries entered a new stage [8–11]. From then on, for just less than ten years, LIBs dominated the market with their excellent electrochemical performance [12]. Nevertheless, with the dramatic development of the electric vehicle (EV) industry, LIBs require enhanced energy density to meet the minimum energy density (~800 W h kg^{-1}) requirements of vehicles [13]. With the development in electrochemistry and material chemistry, conventional graphite-based LIBs widely applied in the industry nowadays are approaching their theoretical energy density [14]. Silicon (Si) is a promising candidate because of the 4200 mAh g^{-1} theoretical specific capacity based on the alloying reaction mechanism to replace the traditional graphite electrode (~372 mAh g^{-1}) [15]. While fully lithiated, 1 Si atom accommodates 3.75 Li$^+$ compared to graphite (LiC$_6$), being theoretically more ideal, along with the improved safety and energy density coming from

its working potential (0.4 V vs. Li/Li$^+$) [16]. Taking lithium cobalt oxide as the cathode and Si anode [17], the reaction for the Si anode is as follows:

$$Cathode: LiCoO_2 \leftrightarrow CoO_2 + Li^+ + e^-$$

$$Anode: 4Si + 15Li^+ + 15e^- \leftrightarrow Li_{15}Si_4$$

$$Overall\ reaction: 15LiCoO_2 + 4Si \leftrightarrow 15CoO_2 + Li_{15}Si_4$$
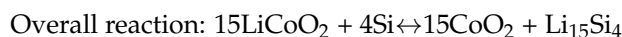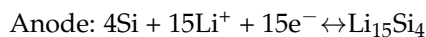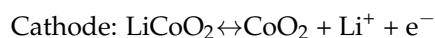
However, with such high expectations, Si also faces challenges, i.e., the well-known more than three-fold volume expansion causes severe pulverization of active substances and electrode decomposition, resulting in the failure of electrochemical performance [18]. Consequently, the huge volume change in Si during cycling also results in uncontrollable stress accumulation and leads to material cracks and capacity decay. The volume effect also causes instability of the battery's internal interface, damaging the solid electrolyte interface (SEI) film and continuously consuming the electrolyte. The SEI film grows thicker to extend the distance of lithium-ion diffusion and weakens the electrical contact between materials with increased impedance and poor rate performance [19,20]. Low reaction kinetics is also a bottleneck issue for Si material because of its semiconducting nature. The rather low electronic conductivity, between 10^{-5} and 10^{-3} S cm^{-1}, and Li ion diffusion rate ($10^{-14}\sim10^{-12}$ cm^2 s^{-1} diffusion coefficient) [21] need improvement to realize high performance.

Researchers have been committed to developing Si materials and their derivatives in the past two decades [22]. Keeping Si's advantages while avoiding the catastrophic volume change is the key for Si to be realistically applied in the LIBs. By reducing the size of Si to submicron level [23], Si can adapt well to volume and stress changes and structural damage can also be reduced [24]. Mixing/compounding/doping Si with rigid or flexible materials (e.g., various forms of carbon and binders) is as effective in improving the cycling stability [25] and energy density since those materials can act as a framework to confine the volume change. Synthesis methods with controllable Si particle shapes and sizes suit the scenario, thus the laboratory-scale Si fabrication and innovation mostly follow the "bottom-up" strategy [26], starting with nano-Si to the fabrication of zero to three-dimensional Si materials and corresponding composites [27]. The classic template-based methods, such as the vapor–liquid–solid and solution-based methods produce Si materials with uniform morphologies and extremely high electrochemical performances [28]. On the other hand, countless up- and downstream compositing strategies can be applied to further enhance the performance at the nanoscale [29]. The mature material modifications have led to undeniable success in the field with numerous research papers and reports. However, the excellent and evolving material design, such as yolk–shell particles and layered structures [30], is at the expense of expensive precursors, complicated protocols, and harsh conditions, limiting the scalability and practicality for mass production. Only a few companies such as Amprius claim the commercialization of high-Si-content LIB anode materials, while the majority of the market still follows a strategy to add a small amount of Si materials to the carbon anode (<20%) to improve the battery performance.

Standing at a perspective to serve the immediate EV market demand, the so-called "top-down" approach is more cost-effective and practical [31]. Most top-down synthesis methods are physical instead of chemical, such as ball milling, laser bombardment, electrospinning, and plasma sputtering [32–34]. The advantage is that it is simple and cost-effective to prepare various exotic three-dimensional structures and porous materials that contain micro- or nanostructures. Electrospinning is a top-down fabrication method that uses strong electric fields to spin polymer solutions or melts in a jet manner to fabricate nanofiber materials. It has been identified as one of the most promising approaches to designing new anode materials and structures. Electrospinning technology is also an effective method to modify silicon carbon materials. The preparation of silicon carbon nanoparticles into nanofibers can effectively slow the volume expansion of silicon after inserting

lithium ions. In addition, mechanical ball milling is commonly used for industrial-scale bulk material grinding and blending. This method uses the grinding balls' kinetic energy to stir and grind the materials, and the materials are dispersed and destroyed to modify the materials during the process [35]. Ball milling is also easily tailored to the current silicon/carbon (Si/C) composite strategy, even though it sacrifices material uniformity, energy density, improved safety, and cycle life [36]. Compared with electrostatic spinning, since the material prepared by ball milling is mostly spherical, which can effectively disperse the stress generated by the volume expansion of lithium inserted in silicon, the material is difficult to fracture due to the uneven stress. Additionally, material prepared by electrostatic spinning almost all have subsequent chemical and thermal treatments [34], which not only increase the complexity of the process, but also increase the cost, and are not conducive to the development of industrialization. Therefore, ball milling is more suitable for the preparation of industrial Si/C anode materials compared to electrostatic spinning.

Although in laboratory synthesis, the top-down ball-milling method is more straightforward to operate than the bottom-up method, the long operation time, noise, difficulty in maintenance, and limited Si morphology hinder the latest research, not to mention the requirement of repetitive trials to improve material uniformity and achieve repeatable results. Thus, there is a gap between the laboratory and industrial scales for ball milling.

This review shares recent progress in laboratory-scale Si, Si/C, and SiO materials synthesized from ball milling, summarizes the protocols and performances, and comments on the feasibility of Si material preparation for industrial operation. With the EV market's rapid growth, the significance of ball milling will greatly increase, and the contents can also be applied to related LIB material production, such as binder materials.

2. Ball-Milling Method

Ball milling is commonly used in industrial mass production for ores, ceramics, and pigments. It mainly uses grinding media to mix and crush material through impact, extrusion, and friction [37]. In the ball-milling process, while the sealed and partially filled chamber rotates along its own longitudinal axis, the grinding balls are given kinetic energy to move at high speed and collide with the materials, realizing samples of desired sizes with increased surface area. While traditional ball milling focuses on physically breaking down and refining material-specific surface area [38], chemical processes (mechanochemistry) are also possible through continuous impact and collision between reactants and balls [39–42]. Unconventional ball-milling protocols, such as cryogenic/magnet milling, can also be adapted for specific situations [43].

The degree of milling, i.e., the material properties after ball milling, are influenced by numerous factors and are typically more complicated than bottom-up synthesis. Milling machine/grinding ball/source material/environmental properties, milling media and time, and ball-to-material ratio need to be considered along with cost and safety for mass production [44]. Continuous operations, such as a coarse mill followed by a fine mill, may further increase the experimental design complexity, and ball milling is usually case by case since various parameters are involved. Laboratory ball milling thus typically analyzes a single variable at a time, while companies have the ability to optimize production in a rather short period at a much higher expense.

Based on the media, two types of ball milling, namely dry and wet, are classified. As the name suggests, wet milling disperses the material in liquid media to form a slurry, while dry milling relies on particle contact. Although dry and wet milling can both be adapted for various materials, certain restrictions do apply. Materials react with liquid such as water should be carried out in a dry environment and inert gas can be used; materials that require rapid mixing and impact are also suitable for dry milling. Pyrotechnic materials possess improved quality using dry milling compared to wet milling. Heavy dust, excess enthalpy, material aggregation/oxidation, and chamber dead volume are the major limitations of dry milling [45–47].

On the other hand, wet milling involves liquid such as water, ethanol, or isopropanol (IPA) to disperse the material and is appropriate for air-free cases. With more uniform material sizes, superior heat dissipation and production efficiency, wet milling suffers from higher costs and extra material post-treatment, such as drying. For Si, both dry and wet millings are reported; the dry method is typically used for laboratory-scale since only a single variable or correlation is the research focus, so other parameters just need to be identical. For example, if milling time vs. Si size distribution is the main focus, other factors such as Si oxidation level or ball sizes are not obstructive to drawing a conclusion once the samples are treated the same during experiments. Additionally, safety and pollution issues for small batch production at the laboratory scale are less of a concern. Industrial-scale Si production typically uses anhydrous ethanol or IPA as the wet-milling media to operate safely, avoid oxidation, and properly store the Si end product before the composite unit.

The choice among ball-milling machine types, high or low energy, should also be decided based on research/production focus, and details about ball-milling basics can be found in other references [48]. This review focuses on the recent advances in ball-milled Si and related materials. It is divided into sections, namely pure Si, Si/C composite, Si/X composite, Si/C/X composite, Si/C composite followed by additional treatments, SiO-based, and other Si-based materials, where X denotes materials mixed and milled in the machine along with Si particles.

3. Pure Si

Pure Si particles, especially nano-Si produced through ball milling, despite the source material size and the milling environment, were soon realized to be not effective compared to bottom-up synthesis because of the reduced material morphology uniformity, size distribution, and the volume change still remained a problem even though the cost was reduced. The research direction turned toward silicon–carbon composites after that [49], and the concept was to rely mainly on carbon materials and add a minor amount of Si; carbon materials also prevent Si volume-change during cycling. This idea is currently commonly applied in industrial Si/C production.

A representative work on the shift from pure Si to Si/C is that by Cetinkaya et al. [50], who studied the effect of carbon content in Si/C through simple and straightforward experiments: 0, 25, and 50 wt% graphite was added to Si during ball milling. Although pure Si showed much higher initial coulombic efficiency (ICE), the discharge capacity soon decayed to < 50 mAh g^{-1}. With increased graphite content, the ICE showed a reasonable decay with > 6 fold cycles and improved discharge capacity, and the higher graphite content of 50% showed increased cycling performance and higher capacity retention of 45% (Figure 1a). Additionally, the X-ray diffraction (XRD) 2θ peak intensity of graphite at around 26.5, 45, and 54° was proportional to the graphite content. While the correlation between battery performance and Si/C composition can be further investigated, it was evident that XRD can be more representative and effective for material evaluation compared to morphology characterizations such as scanning electron microscopy (SEM) for Si material with a large size range. The later research typically involve $< 20\%$ Si content, and recent updates on pure Si are rare.

Not only can XRD reveal Si composite information, the signature peaks also provide valuable information for Si material properties and is thus useful for initial studies to settle the milling parameters at the first stages of ball-milling projects. Typically the first peak, the fcc (111) plane at ~28° 2θ degree, is enough to provide Si particle information such as crystallite size and lattice strain, and milling-time-dependent XRD patterns can be collected and analyzed to form Si-particle-size fingerprints together with SEM images. Gauthier et al. demonstrated that [51] ball-milled micrometric and even near-millimetric silicon have superior electrochemical performance than nanometric Si powders, and one of the major characterization methods was XRD. The broader peaks after milling indicate increased lattice strain and decreased crystallite size (Figure 1b). The milled nanostructured micrometric Si particles contain a large number of dislocations and defects, leading to

different crystallographic planes compared to single-direction commercial nano-Si, contributing to the enhanced electrochemical performance, maintaining a discharge capacity of 1600 mAh g^{-1} after ~600 cycles (Figure 1c). The concept can be used to produce high-performance milled Si materials from large-sized waste Si materials [52,53] to reduce the capital cost, especially for scaled-up processes, while how to incorporate coarse (from bulk to microsized particles) and fine (create nanostructures and decrease material size distribution) milling is properly of great importance.
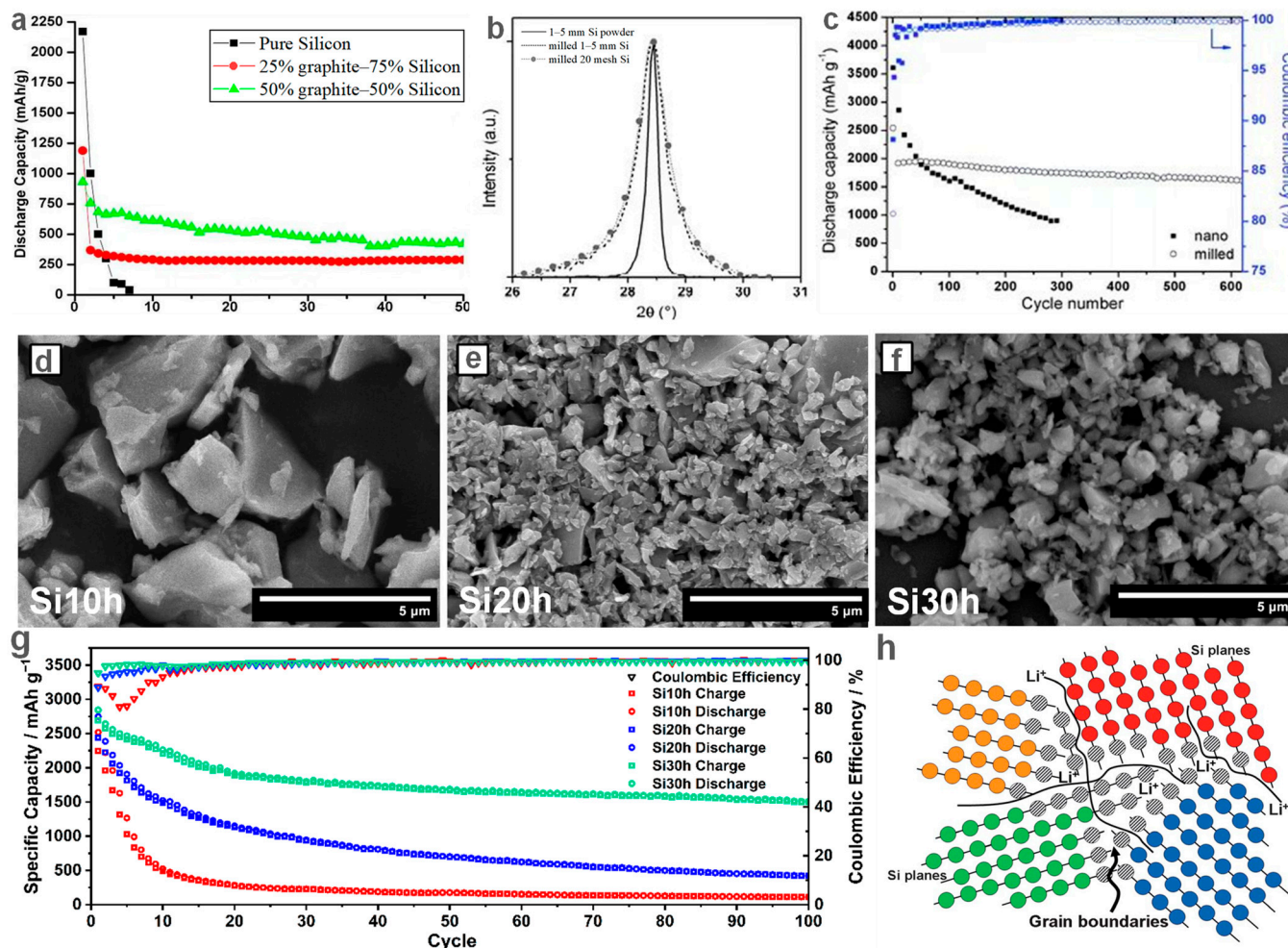

Figure 1. (**a**) Cyclability of 50% graphite–50% silicon [50]. (**b**) XRD patterns of the as-received 1–5 mm Si powder (black line), milled 1–5 mm Si powder (dotted black line), and milled 20 mesh Si powder (dashed gray line with filled circles). (**c**) Discharge capacities and coulombic efficiencies with cycling of milled millimetric Si (O) or nanosized Si-based electrodes for full discharges. Reproduced with permission [51]. Copyright 2013, The Royal Society of Chemistry. (**d**–**f**) SEM images of silicon particles resulting from the ball-milling process for 10 h (Si10h), 20 h (Si20h), and 30 h (Si30h). (**g**) Cycling stability curves of the cells with Si 10h, Si 20h, and Si 30h electrodes at 400 mA g^{-1}. Reproduced with permission [54]. Copyright 2022, MDPI. (**h**) Scheme of the nanocrystalline structure of the milled Si powder showing grain boundaries (hatching) where faster Li diffusion is supposed to occur. Reproduced with permission [51]. Copyright 2013, The Royal Society of Chemistry.

Although pure Si studies were quickly dominated by Si composites, the characterizations, methodologies, and parameter settings have insights into Si-based materials. The time-dependent Si particle shape and size effect was studied by Koraag et al. [54] With increased milling time, the plate-shaped Si was gradually worn to round particles with decreased sharpness, showing isotropic stress and leading to a more stable SEI during cycling (Figure 1d–f). Additionally, the Si size decreased from micro to nano with a narrower

particle size distribution from 10 to 30 h milling, shortening the Li-ion diffusion distance and reducing the crack formation and pulverization, further increasing the SEI stability and cycling performance (Figure 1g).

Pure Si studies typically focus on the experimental condition–particle characteristics–electrochemical performance relations; it is also encouraged to study the detailed reaction mechanism using some common bottom-up techniques, such as transmission electron microscopy (TEM). It was proposed that the additional grain boundaries (interfacial regions) of nanostructured micrometric Si after ball milling that can be regarded as amorphous contributed to the higher electrochemical performance [51] (Figure 1h). Possible future research directions include exploring optimal crystalline/interfacial region content or Li-ion diffusion pattern through the regional network.

Pure silicon nanoparticles prepared by ball milling are still not well adapted to severe volume changes during the insertion/extraction by lithium ions. It has been found in studies that carbon can act as a cushion for volume changes because of its softness, good electronic conductivity, reasonable lithium insertion ability, and small volume expansion [50]. The conclusions from ball-milled pure Si inspired some first-generation Si/C composite fabrication both from top-down and bottom-up [55]. However, caution is needed, especially for pure Si research at the laboratory scale, since the end product may vary greatly even when the same parameters are applied. Bimodal particle size distribution may occur [54], and repeated experiments may be necessary. Additionally, the degree of Si oxidation has to be monitored to draw reliable conclusions.

4. Si/C Composite

Although nanoscale Si can adapt to the volume expansion during cycling, the degradation of Si and the insufficient adhesion lead to anode delamination. Synthesis of Si/C composite follows the strategy to improve the electrochemical performance based on carbon materials with superior conductivity; unlike pure Si synthesis, the attempt was to unleash the maximum energy density from Si. C denotes carbon element-based materials, including graphitizing and nongraphitizing carbons produced from various precursors. Graphitized carbon is a graphitic carbon with a three-dimensional regular ordered structure of graphite. The graphitization of carbon enhances the bulk density, electrical and thermal conductivity, corrosion resistance, and mechanical properties of the product; nongraphitized carbon is the ordinary nongraphitized amorphous carbon. The composite of silicon and carbon can effectively retain the high energy density of silicon and have good electrical and mechanical properties with the addition of various types of carbon [56]. Ball milling is suitable for the material crystal to amorphous transitions at room temperature, especially for Si/C composites.

As early as 1998, Wang et al. reported composites [57] synthesized by ball milling with various graphite/Si atomic ratios. The graphite was grounded and deconstructed, resulting in Si nanoparticle encapsulation by thin amorphous carbon layers. The composite's microstructure contained wrinkled layers with increased interlayer spacings. As the Si content in $C_{1-x}Si_x$ increased from 0 to 0.25, the graphite crystalline size increased while the Si crystalline size decreased. The nanosized Si particles effectively suppressed pulverization during cycling, increasing specific capacity from $437 \, \text{mAh} \, \text{g}^{-1}$ (C_1Si_0) to $1039 \, \text{mAh} \, \text{g}^{-1}$ ($C_{0.8}Si_{0.2}$), even superior to the early graphite/Si composite prepared with a bottom-up chemical vapor deposition method ($500 \, \text{mAh} \, \text{g}^{-1}$) [58]. Although effective, the material's irregularly thick carbon layer and unevenly distributed nano-Si left space for optimization in the ball-milling process and improvement in the electrochemical performance.

Whether dry or wet milling was more effective toward Si/C was discussed by Cabello et al. [59]. Milling with and without IPA as the media were compared. The material morphology of commercial Si source, and dry- and wet-milled Si/graphite was compared using SEM (Figure 2a–c). Both Si and graphite aggregates were observed in the dry sample, leaving voids and dead space in the network, while the graphite remained platelet-like in the wet sample, surrounding and protecting the Si particles. The laminar

graphite survived the lower-friction wet milling and was also helpful during electrode fabrication, contributing to more ordered packing. XRD agreed with the SEM that the wet sample kept well-defined diffraction peaks compared to the poor crystalline structure from the dry sample. Additionally, a higher SiO_x content was confirmed by X-ray photoelectron spectroscopy (XPS) in the dry sample. The ICE increased to 77% for the wet sample compared to the dry sample (66%), and the cycling capacity increased because of the IPA added (Figure 2d). Indeed, for Si-based materials, liquid grinding media possesses advantages in temperature control, safety, and oxidation prevention. However, in this specific research, the IPA was simply added into the milling chamber; the liquid volume and oxygen level should be quantified stepwise, and the heat effect should have been mentioned since pauses were added for heat dispersion and the temperature response could be different for dry and wet milling.

Yoshio et al. provided guidance on the material microuniformity for Si/C composite prepared through ball milling [60]. A footprint to determine the ball-milled Si/C electrode uniformity was proposed—local voltage drop to near 0 V (vs. Li metal) within propylene carbonate containing electrolyte is a sign of electrode dead spot and mechanical failure. Figure 2e shows the disordered graphite flakes damaged during the Li^+ intercalation process compared to the uniform region. The authors also claimed that the grain size holds the key to balancing the electrode uniformity and the material preparation complexity, and Si/C particles with a grain size between 0.5 and 1.0 μm generally present less heterogeneity with higher electrochemical performance when the materials are prepared at a large scale. Note that the particle grain size region can vary based on the raw Si and carbon source and should be tested and optimized case-by-case; this research used synthetic graphite as the carbon source, while currently, more cost-effective sources such as asphalt and others are considered.

Aside from graphite and other conventional hard/soft carbon sources, unconventional carbon sources have also been applied to Si/C composite as well [61]. Multiwalled carbon nanotubes (MWCNT) were used in 1:9, 3:7, and 5:5 MWCNT: Si ratios Figure 2f. The network formed reduced agglomeration for MWCNT and Si separately, and the interspaces and electronic resistance were reduced. With increased MWCNT content, Si shape-change-induced pulverization was suppressed, and the discharge capacity was improved, sacrificing minor ICE. The limitation was that a broader range of MWCNT: Si was not studied, and the composite materials with various ratios did not display obvious morphological differences. The study provided conceptual progress on nanostructured carbon source application into Si/C composite; other nanomaterials, such as nanorods and nanospheres, can also be attempted.

Typically, Si/C composite focuses on the carbon source choice and properties, yet Si material pretreatment and functionalization before ball milling with carbon sources is another effective strategy. It is worth mentioning that graphite-like materials which were prepared by high temperature treatment of unburned carbon concentrates from coal-combustion fly ashes can be used as one of the carbon sources for electrode material in lithium-ion batteries [62]. Fly ashes are the main solid wastes generated in coal combustion plants. If there is an economical and convenient way to separate and further utilize this carbon material as a precursor such as graphite would help reduce the cost of electrode materials for lithium-ion batteries. Zhang et al. [63] introduced amino-functional trialkoxysilanes onto Si particles to modify the Si surface with a -NH_2 group (Figure 2g). Opposite charges were created between Si and graphene sheets to improve the binding efficiency through self-assembly and maintain a uniform Si dispersion between layered graphene sheets with the help of ball milling. The specific capacity cycled at 100 mA g^{-1} was maintained at 1516.23 mAh g^{-1} after 100 cycles, with high capacity retention of 83.28%. The reversible capacity remained at 1151.5 mAh g^{-1} after 1000 cycles, which indicates a decay rate of only 0.08% per cycle, even at 1000 mA g^{-1}. The scaffold graphene structures avoided drastic Si shape change, enhanced the electrode conductivity, and provided faster Li-ion diffusion paths. It is questionable if the separate pretreatments for both Si and

graphene can be easily realized through mass production with proper unit operations and a low cost.
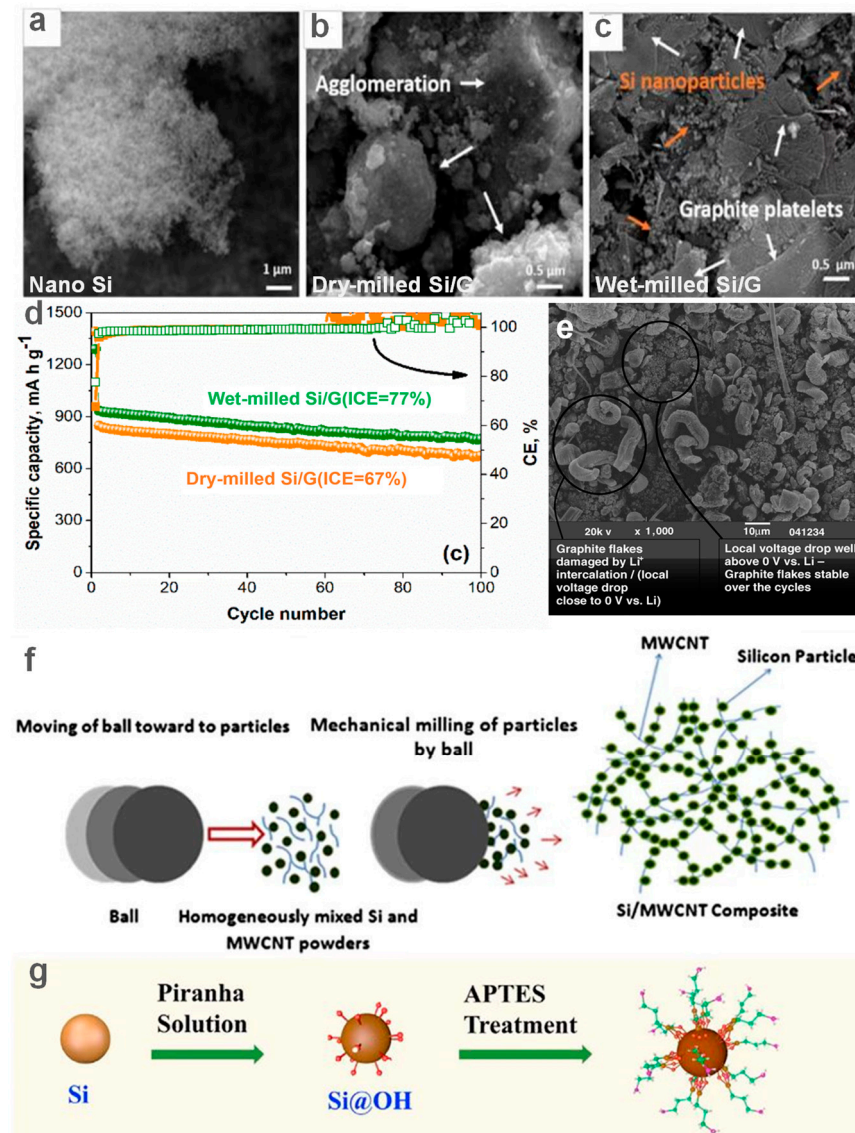

Figure 2. Scanning electron microscopy (SEM) micrographs of (**a**) Si nanoparticles (Alfa Aesar), (**b**) s-BMD, and (**c**) s-BMW. (**d**) Coulombic efficiency (CE) (squares) and specific capacity (spheres) vs. cycle number of e-BMD (orange) and e-BMW (green). The initial coulombic efficiency (ICE) is shown. Reproduced with permission [59]. Copyright 2020, MDPI. (**e**) SEM image of a graphite electrode cycled in 1 M LiPF$_6$ dissolved in propylene–carbonate/ethyl methyl carbonate (PC/EMC) 1:5. Reproduced with permission [60]. Copyright 2022, Elsevier B. V. (**f**) Schematic illustration of the projected nanocomposite structure. Reproduced with permission [61]. Copyright 2013, Elsevier B. V. (**g**) Schematic of the fabrication process of the present Si@APTES/f-Gr composite. Reproduced with permission [63]. Copyright 2021, Elsevier B. V.

Si/C composite through ball-milling possesses improved structural stability and electric conductivity because of the high carbon content and C-surrounding-Si network. At the same time, the achievable capacity decreased because of the low Si content, and it is thus of significance to balance the Si/C content. In addition to the Si source, carbon sources should also be carefully selected before ball milling since the crystallinity, morphology, and other parameters could vary based on the milling time and speed. It is possible to lose the original carbon property, such as high microporosity, and even the desired

material morphology may no long exist after the strong collision for a long time. The related research papers are still mostly performance-oriented since drawing conclusions on materials through characterizations, especially morphological techniques, is difficult. On the other hand, typical control samples for Si/C comparison are pure Si, and the properties of ball-milled carbon sources are not taken into account. Ball-milling Si and the mix with carbon sources followed by additional post-treatments became more reasonable since the Si properties can be controllable, and the carbon quality can be maintained without variation during the grinding.

5. Si/X Composite

Similarly to Si/C, Si/X composite simply changes the carbon source to other materials milled with Si particles in the ball-milling process. The materials typically have additional functions or are superior against Si volume change compared to carbon sources.

Polymer is an outstanding candidate to composite with Si since the long-chain structure can form a network to enfold the Si, and the polymer can also be converted to carbon with various functional groups through pyrolysis if needed. Shi et al. [64] milled micro-Si and poly(vinyl alcohol) (PVA) to a nanostructure in which nano-Si was coated by PVA (Figure 3a). The hydroxyl groups on the PVA chain formed Si-O-C covalent bonds with Si, and the particle size was tunable through PVA weight adjustment. The nanostructure was adaptive to the volume change during LIB cycling, and 5 wt% PVA displayed optimal electrochemical performance. At 0.2 A g^{-1}, the 5 wt% PVA/Si sample provided 1526 mAh g^{-1} capacity after 100 cycles with 86.1% ICE and an average CE of 99.2%. It is obvious from the SEM images (Figure 3b–g) that Si/PVA had ~5 times lower crack width compared to the electrode fabricated with pure Si. The details of the Si/PVA structure were not strongly distributable under TEM, and other polymers with different chain lengths and functional groups can be used for future analysis.

A layered ternary carbide, titanium silicon carbide (Ti_3SiC_2, TSC), was milled with Si to enhance the electrode's mechanical strength and electronic conductivity [65]. Different Ti_3SiC_2/Si mass ratios were applied from 0 to 100 Ti_3SiC_2. The elastic modulus increased as the Ti_3SiC_2 content increased from 1.6 to 18.2 GPa, and material hardness increased from 0.03 to 0.81 GPa. There was also a 5-fold increase in material electronic conductivity. The cycling stability was slightly better because of the Ti_3SiC_2 compared to the pure Si from the rate performance. However, the ICE and cycling performance was inversely proportional to the Ti_3SiC_2 content (Figure 3h). The addition of Ti_3SiC_2 improved the overall mechanical strength by compromising the performance.

Ball-milled Si/iron–manganese alloying behavior was studied in depth by Cao et al. [66] Having similar atomic radii, Fe and Mn silicides show different structures and the ternary system properties were investigated for the first time for LIB anodes. On the $Si_{85}Fe_{15}$-$Si_{75}Mn_{25}$ tie line, alloys involve Si, Si_2Fe, and $Si_{19}Mn_{11}$ (Figure 3i). Ball milling showed its advantage in preparing large quantity samples with various mixing ratios simultaneously. $Fe_xMn_ySi_{100-x-y}$, where x and y are 5/0, 12/5, 9/10, 6/15, 3/20, and 0/25, were prepared, and three regions of phase behaviors were concluded from fitting XRD results (Figure 3j). Amorphous Si was observed in $Fe_{15}Si_{85}$ along with β-$FeSi_2$ and α-$FeSi_2$. The CE decreased with the increase in Mn content because of the exaggerated electrolyte decomposition, even though the volume expansion was less severe. The study of Si/Fe-Mn was an excellent example of a laboratory-scale ball-milling application to explore the alloy-mechanism performance correlation and can also be applied to other alloy combinations.

Materials other than carbon-based may make up some of the advanced properties carbon sources cannot provide, yet the material selection needs additional consideration. Researchers need to take into account the mechanical properties, material reactivity with Si, the milling media, and even the balls before milling to avoid safety issues and then obtain materials with enhanced properties for LIB anodes. Situations such as Ti_3SiC_2 may occur, where ball-milled material properties were improved but not helpful to the electrochemical performance. Thus, there are fewer Si/X composites with the abovementioned rather strict prerequisites.
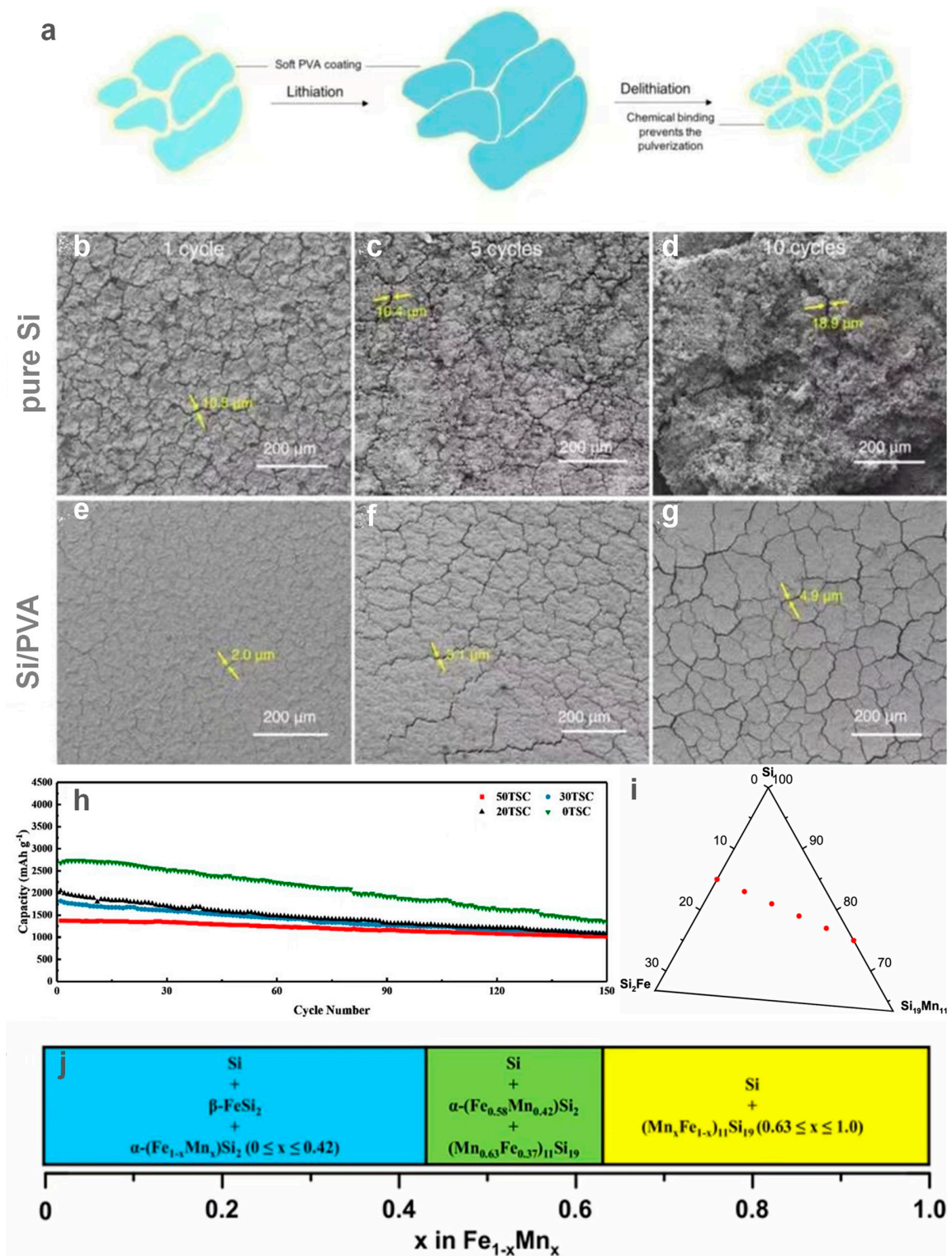
Figure 3. (**a**) Schematic diagram of the lithiation/delithiation process of the ball-milled silicon materials; morphology of cycled silicon electrodes. SEM images of (**b**–**d**) high-energy ball-milling (HEBM) Si electrodes and (**e**–**g**) reactive high-energy ball-milling (RBM) Si-5% PVA after (**b**,**e**) one, (**c**,**f**) five, and (**d**,**g**) 10 cycles, respectively. Reproduced with permission [64]. Copyright 2020, American Chemical Society. (**h**) Cyclic performance of Si/TSC with different mass ratios of TSC. Reproduced with permission [65]. Copyright 2019, Elsevier B. V. (**i**) Composition of ball-milled samples overlaid on a truncated Fe–MnSi ternary phase diagram. (**j**) The observed phase behavior during ball-milling compositions along the $Si_{85}Fe_{15}$–$Si_{75}Mn_{25}$ tie line [66].

6. Si/C/X Composite

The experimental logic flows smoothly from Si/C and Si/X to the combination of Si/C/X; the ternary system gathers the advantages from the three components and boosts the LiB performance to a higher level, ideally. Additionally, precursors with various shapes and morphology can be synthesized and milled with other materials.

Compounds with great hardness (B_4C, TiC, TiB_2) were typically applied to help lower Si grain size in a shorter period. However, other product characteristics, especially electric conductivity, were not considered. Different ratios of TiB_2 and Si were milled with the addition of graphite after 8 h of milling at a speed of 500 rpm [67]. The hard TiB_2 turned both Si and graphite amorphous, forming core-shell structures in which Si was sandwiched between the outer carbon shell and the TiB_2 core. Nanoscale Si/TiB_2/G with a molar ratio of 4:3:3 showed a superior performance of 660 mAh g^{-1} for 60 cycles. An optimally low TiB_2 did not prevent electron/Li-ion transfer to the Si, leaving dead space so that Li-ion cannot reach the Si. However, with an increased TiB_2 molar ratio, minor cracks form to activate the trapped Li-ion, leading to enhanced capacity. The molar ratio of the three components along with the sequence of material addition during ball milling can be investigated in detail to improve the performance. A similar work [68] on Si/TiC/G followed different protocols and synthesized TiC through ball milling before the composite process. The main focus was the effect of milling time on the material instead of the mixing ratio and the rotational speed was kept at either 1000 or 600 rpm. The situation became more complex with multiple scenarios when the Si and TiC were milled for short/long time. When the milling time was 2 h, the Si maintained its crystallinity and was in a mixture form with TiC. On the other hand, Si became amorphous after milling with hard TiC (Figure 4a). The Si/TiC/G milled for 10 h showed improved and more stable cycling performance with the help of the 2–15 nm well-spread conductive TiC network, and the battery retained 835.4 mAh g^{-1} over 100 cycles (0.2 C, 71.5% capacity retention), as shown in Figure 4b. The combination of the two studies provides a comprehensive view of the Si/C with the addition of materials with high hardness.

Ball milling can serve as a proper industrial waste treatment and recycling tool. Si/C/binder composite proposed by Sbrascini et al. [69] utilized corn-cob-derived hard carbon (CCDHC) as the carbon source (Figure 4c). Combined with chitosan/citric acid (CS/CA) crosslinked binder, the hard carbon matrix maintained excellent electrode and SEI integrity, leading to higher cycling stability and capacity retention compared to other binders (Figure 4d). This study provides insights into tailoring ball milling with up- and downstream processes to reduce the capital cost and investment further.

While binary composite typically follows the route of Si-wrapping, different morphologies such as layered, sandwich, and core-shell are possible for the ternary composite. Mesoporous Si was sandwiched between SnO_2 and N/P doped graphitic carbon to form a C/Si@SnO_2 structure [70] (Figure 4e). It was claimed that Si was oxidized, and the Si-O-C and Si-O-Sn bonds formed through Si integration promoted Li-ion diffusion since additional mesopores and cracks were formed during cycling, which allowed fast charging performance with a discharge capacity of 805.57 mAh g^{-1} at 0.2 A g^{-1} for ~ 500 cycles and maintaining 919.21 mAh g^{-1} 1 at 0.1 A g^{-1} for 200 cycles (Figure 4f). The structure should have been denoted as C/SnO_2@Si since the as-formed SiO_x layer was the coating layer, and milled pure Si performance should be provided as a comparison.

Pretreatment of the milling precursors is also common to realize the final product with superior electrochemical performance. Material oxidation through heating effectively introduces lithium oxide (Li_2O) and lithium silicate species during cycling, buffering the Si volume expansion [71]. Cu-Zn nanomaterials were heated and milled with Si/C to form Si/Cu-Zn(ox)/C composite; a Cu-rich Cu_xZn matrix was generated along with ZnO, CuO, and C to improve the electronic conductivity. During the first discharge process, the electrode was further activated since the metal oxides were transformed into Li_2O, Cu, and Zn, leading to a specific capacity of 800 mAh g^{-1} cycled 100 times and only 20% capacity loss cycled with rates from 0.1 to 1 A g^{-1}. Similar heat treatment, although conducted with

a much higher temperature, 900 °C, was performed for Si [72], followed by hydrofluoric acid etching to create Si/SiO$_x$ composite followed by ball milling with graphite to form Si/SiO$_x$/G with promoted electrochemical performance, using SiO$_x$ as the buffer layer and graphite as the connecting medium between the Si-based material and the current collector.

While more advanced than the Si/X binary systems, synthesizing Si/C/X can be more complicated, with increased possibilities from countless pretreatments and milling sequences. Single or multistep ball milling may be involved, and the material characteristics may vary because of the protocol. Even minor operations such as product collection could greatly affect the oxidation extent. Thus, repeatable and reliable experimental design is necessary when more than one material is added to the milling process.
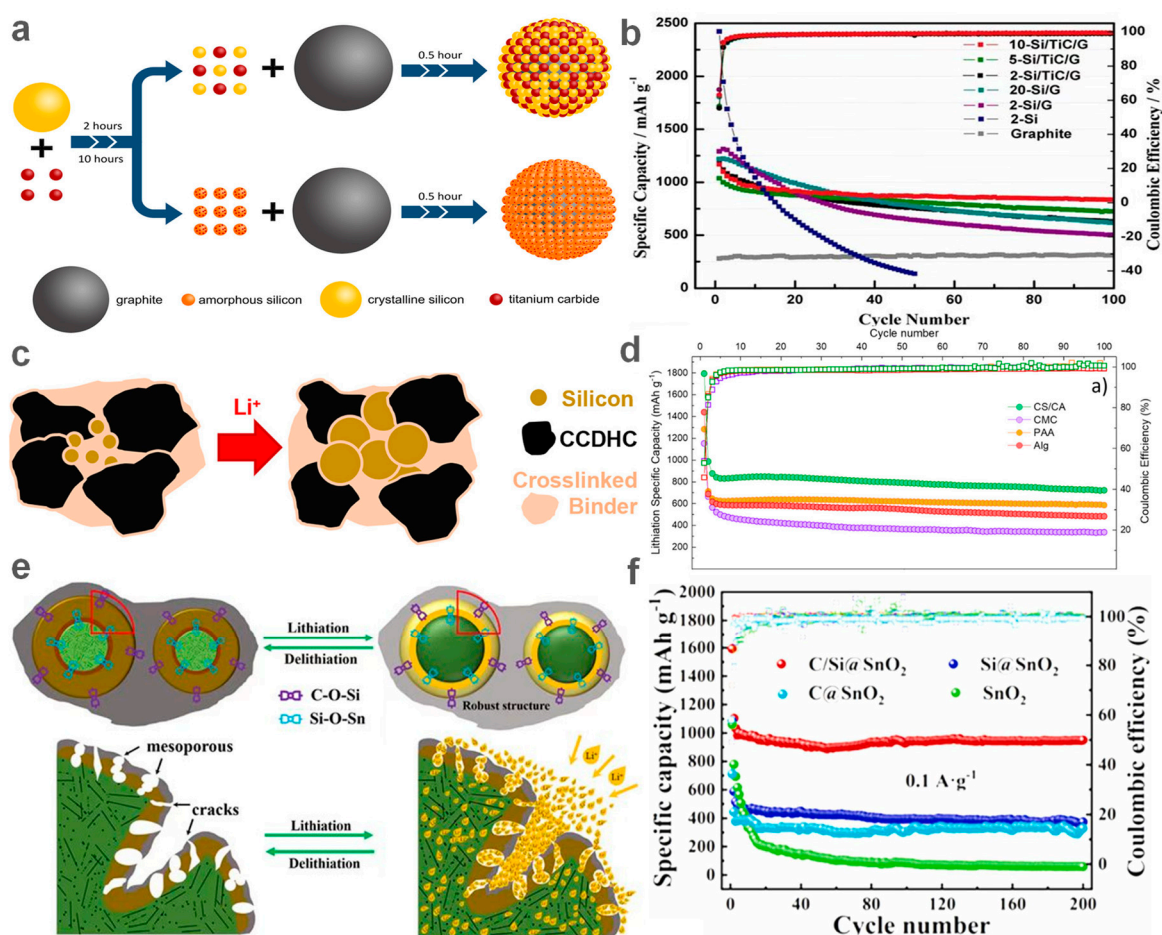

Figure 4. (**a**) Schematic of the preparation processes of Si/TiC/G composites. (**b**) Cycle performance of Si/G and Si/TiC/G electrodes with different ball-milling times at 0.2 C. Reproduced with permission [68]. Copyright 2021, Springer Nature. (**c**) Schematic diagram of working volume change in Si/CCDHC composite. (**d**) Comparison of galvanostatic cycling of Si/CCDHC employing different binders at 1.0 A g^{-1} (CS/CA = green, sodium carboxymethyl cellulose (CMC) = violet, polyacrylic acid (PAA) = orange, sodium alginate (Alg) = red). Reproduced with permission [69]. Copyright 2022, American Chemical Society. (**e**) Reaction mechanism diagrams and diagram of Li$^+$ diffusion of the C/Si@SnO$_2$. (**f**) Cycle curves of C/Si@SnO$_2$, Si@SnO$_2$, C@SnO$_2$, and SnO$_2$ electrodes at 0.1 A·g^{-1}. Reproduced with permission [70]. Copyright 2022, Elsevier B. V.

7. Si/C Composite Followed by Additional Treatments

Rather than Si/C/X composite, which focuses on the milling and material treatment processes, a more popular strategy is to add one or more post-treatments to Si. Moreover, ball milling only serves a section of the overall process. Although it sounds complicated, the protocol typically involves industrially mature techniques such as solution etching,

material mixing, and heating and spray drying, which is especially suitable for large-scale Si material synthesis with low operational cost and labor requirements. Another important concept to note is that the carbon sources are typically specified in this section compared to the formerly mentioned categories. A common approach uses graphitizing carbon to serve as the capacity source along with Si because of its higher density and ordered structure. Nongraphitizing carbon is used as the protection/buffer layer to suppress volume change through its low density and high porosity nature. As a result, Si/G/C composite is usually denoted, and since most of the recent Si ball-milling studies involve post-treatments, there are more scientific reports than other strategies.

Laboratory-scale studies still focus heavily on the source material and ball-milling parameters, followed by simple post-treatments. A Si/G composite followed by poly-acrylonitrile (PAN) coating was prepared, and the PAN served as the carbon source and support after heating and NaOH etching [73] (Figure 5a). The NaOH etching process was claimed to remove certain Si to buffer the volume expansion. The etched-Si/G/C composite outperformed the Si/G/C at a low current density and for rete performance, yet the specific capacity was lower at a high current density; an in-depth investigation is needed for proper explanations. A similar approach was taken in [74], yet the composite materials were reversed. Cyclized PAN was ball milled with Si and graphite in a single batch and then carbonized, and graphite served as the wrapping network. This reversed Si/amorphous carbon/graphite structure displayed more stable cycling performance but lower discharge capacity during the initial cycling period, and the performance variation is possibly attributed to NaOH etching.

Si/MWCNT with heat-annealing treatment was studied by Nulu et al. [75]. In addition to the CNT network, the mild annealing temperature at 400 °C promoted Si to attach to the outer wall of MWCNT with minor aggregations without Si oxidation. Additionally, the mild oxidation of the CNT wall created additional surface defects to promote the electrochemical performance, realizing discharge capacities of 1685 mAh g^{-1} at 1 C for more than 80 cycles and 913 mAh g^{-1} at 5 C for > 100 cycles. Similarly, another work reported the modification of Si/TiN/C by calcination and citric acid etching [76]. A highly porous composite was synthesized, adapting the high electrode integrity and electric conductivity provided by TiN. It was claimed that the composite exhibited high stability in a wide temperature range (5–50 °C) in addition to excellent cycling performance; in fact, the reversible specific capacity dropped under 200 mAh g^{-1} when the temperature was below 15 °C. Post-treatments, especially thermo-treatments, allow low-cost industrial waste-derived hydrocarbon sources to composite with Si particles. Waste petroleum resin derived from crude oil with the formula $C_{176}H_{148}O$ containing 92.5 wt% C, 6.0 wt% H, 0.6 wt% O, and minor N and S was ball milled with Si [77]. The Li_2O volume expansion buffering effect was correlated to the surface Si oxidation state and was greatly influenced by the calcination temperature. A calcination temperature of 700 °C showed the highest battery performance of 2291 mAh g^{-1} first cycle discharge capacity and retained 76% of the capacity after 100 cycles with the initial capacity of 1402 mAh g^{-1}. A cost analysis comparing the waste resin to regularly used carbon sources may be more convincing to promote the material application.

In situ mechanochemical reduction was realized when micro-Si was milled with nano-SnO_2 [78], SnO_2 was reduced, and Si was partially oxidized to SiO_x; the as-formed Si/Sn@SiO_x composite was then coated with thin carbon layers using chemical vapor deposition. The combined top-down and bottom-up strategy achieved exceptional rate performance with a high-capacity retention of 95% even after 500 cycles 2 A g^{-1} (<0.01% capacity loss per cycle) because of the synergistic buffer effect from the carbon coating and the SiO_x.

Caution is needed with Si/C post-treatments when collecting the ball-milled products after dry milling. Oxidation may be induced in Si or even composite materials when the product is collected from dry milling, leading to unexpected battery performance

fluctuation; on the other hand, how to effectively remove the liquid media for Si material through wet milling is an issue.

Rapid solvent-removing techniques such as spray-drying are outstandingly effective in drying and reshaping the Si-based materials, making them ready for anode fabrication or the next composite step. Hierarchical silicon/reduced graphene oxide/C was prepared by Wu et al. [79]. Pretreated positively charged Si with a thin SiO_x layer was milled with negatively charged graphene oxide (GO) and carbon sources and spray-dried with polystyrene spheres as the sacrificial template; the Si/GO/C was then sintered to form the Si/rGO/C composite (Figure 5b). The spherical composite contained <50 nm mesopores to provide a fast Li-ion transport path and mitigate the Si volume change. The spray-dried Si/GO/C displayed a much more uniform spherical morphology than most references mentioned above. High capacity retention of ~75% was achieved, while the pristine Si only had 40% capacity retention. It is noticeable that cycling involves a rather large capacity fluctuation, which can be attributed to the complex structure. This approach is close to the most adapted Si/C production procedures, except that multiple pretreatments and costly precursors were used.

Du et al. [80] vividly depicted their dual-layered Si/C composite as "pearl in mussel", in which Si was firstly embedded into the glucose-based carbon source and additional graphite was introduced. Similar to the previously mentioned strategies, the amorphous carbon from glucose milling and calcination, along with the rigid graphite, ensured a high performance of 670 mAh g^{-1} specific capacity and 85% capacity retention for >850 cycles at 0.2 C. Like other organic sources, glucose serves as an easy-to-obtain and inexpensive carbon source, yet the calcination temperatures and functional groups require further investment to improve the battery performance further.

Other post-treatments also show excellent effectiveness for Si/C composite to realize performance-beneficial morphologies. Aside from the mostly adapted high-temperature annealing processes, unconventional post-treatment of the ball-milled Si material under high pressure was investigated [81]. Si/CNT/G composite was treated with a supercritical CO_2 fluid under 12 MPa at 70 °C, causing the exfoliation of graphite to folded graphite. Si particles were homogeneously distributed between the folded graphite layers. The graphite scaffold prevented Si from directly contacting the electrolyte while retaining a high electric conductivity with the help of the CNT, leading to improved cycling performance of 970.3 mAh g^{-1} with 0.2 A g^{-1} current density for more than 100 cycles. Porous silicon is typically synthesized through hydrofluoric acid etching, which is not safe to realize with the ball-milling process, thus is difficult to scale up. Dong et al. used a ball-milling-friendly approach: LiCl [82] was used as a removable template to mill with Si particles and washed away after compositing and calcinating, creating mesopores around 12.8 nm, leading to improved cyclability compared to pure Si and nonporous Si/C anodes. Similar to spray drying, other approaches can realize Si/C with controllable and rather uniform Si/C morphologies. Microspherical Si/C containing nanostructures were synthesized via softening and polycondensation of pitch powder [83]. The pitch powder, Si nanoparticles, and graphite flakes were milled in unconventional poly(dimethylsiloxane) media and stirred with elevated temperature and pressure. The spherical shape with compact structure allowed for increased tap density and electrode mechanical properties, leading to a high ICE of 90.5% and an 85% capacity retention over 300 cycles at a high areal capacity of 4 mAh cm^{-2}. Additional treatments, such as chemical activation, deserve further investigation.
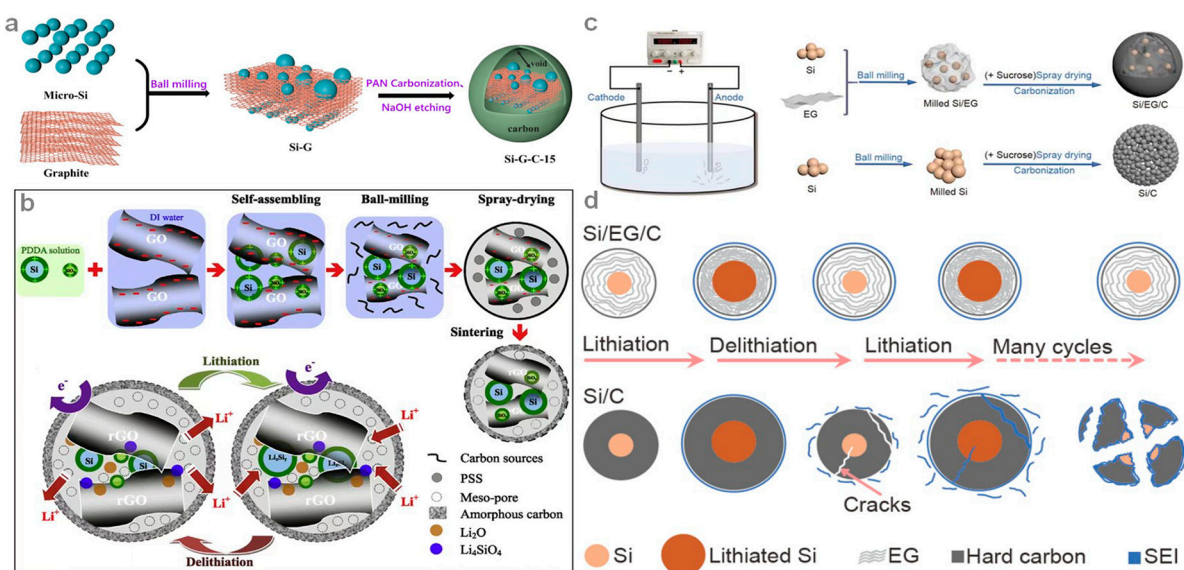
Figure 5. (**a**) Schematic diagram of Si-G-C-15 sample synthesis process. Reproduced with permission [73]. Copyright 2022 Elsevier B. V. (**b**) Synthesis procedure of the ternary hierarchical Si/rGO/C composite microsphere and schematic diagram of electron (e^-), Li-ion (Li^+) pathways, and synchronous formation of inert products such as Li_2O and Li_4SiO_4, which can not only act as disperse media to prevent from Si aggregation, but also serve as buffer matrix to tolerate the volume changes in Si nanoparticles (SiNPs), in the Si/rGO/C composite microsphere during the first lithiation process. Reproduced with permission [79]. Copyright 2019, Elsevier B. V. (**c**) Schematic illustration of the apparatus of the electrochemical exfoliation of graphite rods and the preparation process for Si/EG/C and Si/C. (**d**) Schematic illustration of Si/C and Si/EG/C during a charge–discharge cycle. Reproduced with permission [84]. Copyright 2022, Springer Nature.

8. SiO-Based Materials

Reading through the previous sections, it should be rather clear how different researchers engage in the Si anode problem—suppressing Si volume, improving electrical conductivity, and Li-ion diffusion rate, while sticking tightly to the ball-milling method. A certain amount of SiO_x buffers the Si volume change by forming Li_2O and lithium silicate species, sacrificing the ICE for cycling stability. However, too large an oxidization content also leads to low electrical conductivity and specific capacity; the details about SiO_x are well explored and explained in previous research [85,86].

For most of the ball-milled Si-based research, it is not easy to maintain an oxygen-free environment, yet usually the SiO_x effect was ignored, and only a few studies characterized the oxygen content. At the same time, most ball-milled SiO-based material papers follow the logic discussed above [87–94], except for switching commercial Si to SiO_x and composite material sources, while few provide material oxidation status study through the ball-milling process and insights into the next-generation ball-milled SiO_x research direction. Unlike the studies using commercial SiO_x starting material, several studies analyzed the oxidation level through ball milling. Hwang et al. mixed and milled Si and SiO_2 and investigated the correlation between milling time and the SiO_x oxidation status, decoupled and fitted XPS results of the milled sample served as a powerful indicator and was compared to commercial SiO [95]. Park et al. [96] milled Si with ZnO to form Zn and SiO, and the Zn was etched away to form porous SiO to enhance the anode properties.

Different from Si, some biodegradable materials naturally contain SiO_x. In addition to particle size refinement and crystal–amorphous transformation, ball milling holds an unparalleled advantage in Si-based material composition redistribution and dispersion with large quantities. Ball milling is especially suitable for pairing with the idea of sustainable, biodegradable natural resources. Feng et al. [97] proposed the idea of a SiO_2/C composite prepared from rice husks. Partially oxidized Si particles were demonstrated to help improve

LIB electrochemical performance, and the SiO_2 distribution was controllable and correlated to the milling time. While the natural SiO_2 in rice husks had SiO_2 aggregation issues and materials ground with a long duration showed greatly varying particle size distribution, SiO_2/C milled for 12 h showed advanced performance of 827 mA h g^{-1} for 300 cycles with 100 mA g^{-1} current density. The concept provides insights into environmentally friendly bulk material production for LIB, and additional parameters other than milling time, such as raw materials used, additives to pair with the raw materials, and rotational speed vs. particle size distribution can be studied to promote the idea.

9. Other Si-Based Materials

With Si and SiO being the most popular ball-milling candidates, other Si-based materials, analyses, and methodologies existed to promote a more comprehensive understanding. SiP-based materials [98–101] have also been brought to attention because of their high theoretical capacity (2900 mAh g^{-1}). Researchers have focused on the relationship between the as-prepared Si anodes to other LiB battery parts, such as binder materials [102]. Processing-related studies such as material doping were also investigated to understand material synergetic effects [101,103]. Table 1 summarizes the detailed LIB electrochemical performance for most of the ball-milled materials discussed above, while the few that did not provide enough performance information were excluded.

Table 1. Summary of recent ball-milling-based Si materials for LIB.

Material	Current Density (mA g^{-1})	ICE (%)	Reversible Capacity (mAh g^{-1})	Cycle Number	Year	Ref.
50:50 wt% Gr/Si	300	/	418.5	50	2012	[50]
Milled Si	/	81	1600	600	2013	[51]
Si/CNT	400	98.06	1761	100	2022	[54]
Si/C	45	/	1039	20	1998	[57]
Wet Si@Graphite	250	77	850	100	2020	[59]
Si/MWCNT	200	66	750	30	2013	[61]
Si@APTES/f-Gr	1000	61.23	1151.5	1000	2021	[63]
Si-5% PVA	200	86	1526	100	2020	[64]
Si/TiB$_2$/C	100	71.7	662	60	2015	[67]
Si/TiC/Graphite	1500	/	501.5	300	2021	[68]
Si/Corn Cob-carbon	1000	53.24	800	1800	2022	[69]
C/Si@SnO$_2$	100	77.96	919.21	200	2022	[70]
Si/Cu-Zn(ox)/Cu	200	50	800	100	2021	[71]
Si/SiO$_x$/Graphite	100	62.2	804.2	100	2020	[72]
Si-Graphite-Carbon	200	/	965	100	2022	[73]
Si@c-PAN@G	200	83	1422	50	2019	[74]
SiCNT	1 C	83.7	1685	80	2020	[75]
nano-Si/TiN@carbon	500	71.4 (100 mA g^{-1})	852.82	800	2019	[76]
CPC/Si	0.1 C	80.5	1402	100	2021	[77]
Si/CNTs@FG	200	62.3	1204	100	2020	[81]
Si/rGO/C	400	/	602	500	2019	[79]
Si/C	200	89.4	670	850	2021	[80]
Porous Si@C	0.2 C	76.4	680	50	2021	[82]
Si/EG/C	500	85	834	500	2022	[84]
SiO$_x$/Ag/C	0.5 C	71.5	1102.7	150	2021	[87]
SiO$_x$/G/SnO$_2$	100	62.2	424.6	110	2022	[88]
SiO$_x$/C@CoO	1000	68.1	1079	250	2019	[89]
C nanoslices-SiO$_x$	1000	66.1	900	600	2021	[90]
SiO/C-nanofiber	0.1 C	35.7	700	200	2011	[91]
Si@SiO$_2$@C	1000	54	973	200	2021	[92]
SiO$_x$@C(SC)	200	/	729.5	200	2021	[93]
SiO@TiO$_2$	200	79.4	901	200	2019	[94]
SiO$_x$	100	71.7	1270	100	2019	[95]
SiO	100	48.9	783	200	2020	[96]
SiP$_2$/nanocarbon	500	88 (100 mA g^{-1})	1515	300	2019	[98]
CuSi$_2$P$_3$@G	2000	/	1394	1500	2021	[99]
ZnSi$_2$P$_3$/C	300	92	1955	500	2019	[100]
AlSiP	100	/	1580	30	2023	[101]
Si/Graphene	400	84.6	484	50	2014	[102]
SiO@C/CNS	1000	51 (100 mA g^{-1})	690	400	2021	[103]
Si/Sn@SiO$_x$-C	2000	71.8	1073	500	2021	[78]
SiO$_x$/C	100	/	550	180	2019	[104]
Fe$_{14}$Si$_{86}$	0.5 C	92 (0.1 C)	/	100	2020	[105]
BG/Si	500	82.5	1110	100	2021	[106]

10. Conclusions and Outlook

This review summarized the recent progress in ball-milled Si-based anode materials for lithium-ion batteries. Ball milling serves as a low-cost, easy-to-operate method for Si mass production. The core concept and key issues need to be resolved—how to minimize Si volume change while promoting the material, electrical conductivity, and Li-ion diffusivity in a rather uncontrollable mixing and grinding process, where uncertainty occurs even when a single parameter or operation varies.

We have categorized the research into material-based sections to better represent the strategic evolution to ball-mill Si materials. Currently, one of the most adapted protocols is compositing Si with graphitic carbon and then coating the material with amorphous carbon. The Si/G provides enhanced specific capacity, and the amorphous coating suppresses the Si volume change and provides paths for Li-ion diffusion. Additionally, both carbon layers provide high electrical conductivity.

Compared to the dominating bottom-up methods, ball milling, as one of the top-down syntheses, still remains a minority because of the progress/operation-oriented research focus, time-consuming experiments, entangled and complicated variable relations, and the high investment and safety concerns at the laboratory scale. More importantly, a long project cycle may only lead to a small increase in the electrochemical performance, making ball milling less worthwhile for performance-oriented research.

However, from an industrial perspective, facing a drastically growing electric vehicle market where even a 5% increase in the LIB energy density means market domination, ball-milling Si becomes one of the most promising methods. Mature ball-milling technology requires little initial investment, and the long project cycle can be effectively reduced by employing multiple machines simultaneously. Thus, ball-milling Si anode is one of the sweet spots for LIB-related industries and will attract increased attention in the near future. Unfortunately, the gap between laboratory- and industrial-scale ball-milled Si may increase because of the increasingly mature ball-milling protocol, leading ball-milled Si research toward a more profit-oriented optimization path.

References

1. Zhang, Y.; Zhou, C.-G.; Yang, J.; Xue, S.-C.; Gao, H.-L.; Yan, X.-H.; Huo, Q.-Y.; Wang, S.-W.; Cao, Y.; Yan, J. Advances and challenges in improvement of the electrochemical performance for lead-acid batteries: A comprehensive review. *J. Power Sources* **2022**, *520*, 230800. [CrossRef]
2. Islam, J.; Anwar, R.; Shareef, M.; Zabed, H.M.; Sahu, J.N.; Qi, X.; Khandaker, M.U.; Ragauskas, A.; Boukhris, I.; Rahman, M.R.; et al. Rechargeable metal-metal alkaline batteries: Recent advances, current issues and future research strategies. *J. Power Sources* **2023**, *563*, 232777. [CrossRef]
3. Zhao, Z.; Liu, B.; Shen, Y.; Wu, T.; Zang, X.; Zhao, Y.; Zhong, C.; Ma, F.; Hu, W. Comparative study of intrinsically safe zinc-nickel batteries and lead-acid batteries for energy storage. *J. Power Sources* **2021**, *510*, 230393. [CrossRef]
4. Wang, C.; Mu, X.W.; Yu, J.M.; Lu, Z.D.; Han, J. Scalable hierarchical lithiophilic engineering of metal foam enables stable lithium metal batteries. *Chem. Eng. J.* **2022**, *435*, 134643. [CrossRef]
5. Zhang, Y.; Zuo, T.-T.; Popovic, J.; Lim, K.; Yin, Y.-X.; Maier, J.; Guo, Y.-G.J.M.T. Towards better Li metal anodes: Challenges and strategies. *Mater. Today* **2020**, *33*, 56–74. [CrossRef]

6. Wang, X.S.; Zhuang, J.C.; Liu, M.Z.; Wang, C.; Zhong, Y.T.; Wang, H.R.; Cheng, X.Q.; Liu, S.; Cao, G.Z.; Li, W.S. Facile and scalable engineering of a heterogeneous microstructure for uniform, stable and fast lithium plating/stripping. *J. Mater. Chem. A* **2019**, *7*, 19104–19111. [CrossRef]

7. Ren, Y.X.; Zhao, T.S.; Jiang, H.R.; Wu, M.C.; Liu, M. A stabilized high-energy Li-polyiodide semi -liquid battery with a dually-protected Li anode. *J. Power Sources* **2017**, *347*, 136–144. [CrossRef]

8. Sun, S.; Wang, C.; Wang, Q.-C.; Liu, Y.; Xie, Q.; Zeng, Z.; Li, X.; Han, J.; Guo, R. Three-in-one oxygen-deficient titanium dioxide in a pomegranate-inspired design for improved lithium storage. *J. Colloid Interface Sci.* **2023**, *633*, 546–554. [CrossRef]

9. Yan, J.; Zhao, X.; He, S.; Huang, S.; Qin, H.; Lou, H.; Hou, X. Artificial solid electrolyte interphase coating to reduce lithium trapping in silicon anode for highly stable lithium storage. *Surf. Interfaces* **2022**, *31*, 102029. [CrossRef]

10. Jeon, Y.; Kim, J.; Jang, H.; Lee, J.; Kim, M.G.; Liu, N.; Song, H.-K. Argentophilic pyridinic nitrogen for embedding lithiophilic silver nanoparticles in a three-dimensional carbon scaffold for reversible lithium plating/stripping. *J. Mater. Chem. A* **2022**, *10*, 1768–1779. [CrossRef]

11. Han, X.; Zhang, Z.; Chen, H.; Luo, L.; Zhang, Q.; Chen, J.; Chen, S.; Yang, Y. Bulk boron doping and surface carbon coating enabling fast-charging and stable Si anodes: From thin film to thick Si electrodes. *J. Mater. Chem. A* **2021**, *9*, 3628–3636. [CrossRef]

12. Nitta, N.; Wu, F.; Lee, J.T.; Yushin, G.J.M.T. Li-ion battery materials: Present and future. *Mater. Today* **2015**, *18*, 252–264. [CrossRef]

13. Li, W.D.; Erickson, E.M.; Manthiram, A. High-nickel layered oxide cathodes for lithium-based automotive batteries. *Nat. Energy* **2020**, *5*, 26–34. [CrossRef]

14. Liao, Y.Q.; Wu, C.; Zhong, Y.T.; Chen, M.; Cai, L.Y.; Wang, H.R.; Liu, X.; Cao, G.Z.; Li, W.S. Highly dispersed Co-Mo sulfide nanoparticles on reduced graphene oxide for lithium and sodium ion storage. *Nano Res.* **2020**, *13*, 188–195. [CrossRef]

15. Ryou, M.H.; Kim, S.H.; Kim, S.W.; Lee, S.Y. A microgrid-patterned silicon electrode as an electroactive lithium host. *Energy Env. Sci.* **2022**, *15*, 2581–2590. [CrossRef]

16. Das, S.; Shamim, S.U.D.; Hossain, M.K.; Ahmed, F.; Hossain, M.A.; Rahman, M.O. A novel silicon-doped 2D Ti2C MXene monolayer as high capacity stable anode material for lithium ion batteries: Insight from density functional theory study. *Appl. Surf. Sci.* **2022**, *600*, 154173. [CrossRef]

17. Thackeray, M.M.; Wolverton, C.; Isaacs, E.D. Electrical energy storage for transportation-approaching the limits of, and going beyond, lithium-ion batteries. *Energy Env. Sci.* **2012**, *5*, 7854–7863. [CrossRef]

18. Liu, N.; Lu, Z.; Zhao, J.; McDowell, M.T.; Lee, H.-W.; Zhao, W.; Cui, Y. A pomegranate-inspired nanoscale design for large-volume-change lithium battery anodes. *Nat. Nanotechnol.* **2014**, *9*, 187–192. [CrossRef]

19. Zuo, X.X.; Zhu, J.; Muller-Buschbaum, P.; Cheng, Y.J. Silicon based lithium-ion battery anodes: A chronicle perspective review. *Nano Energy* **2017**, *31*, 113–143. [CrossRef]

20. Han, X.; Zhou, W.; Chen, M.; Chen, J.; Wang, G.; Liu, B.; Luo, L.; Chen, S.; Zhang, Q.; Shi, S.; et al. Interfacial nitrogen engineering of robust silicon/MXene anode toward high energy solid-state lithium-ion batteries. *J. Energy Chem.* **2022**, *67*, 727–735. [CrossRef]

21. Shen, D.Z.; Huang, C.F.; Gan, L.H.; Liu, J.; Gong, Z.L.; Long, M.N. Rational Design of Si@SiO$_2$/C Composites Using Sustainable Cellulose as a Carbon Resource for Anodes in Lithium-Ion Batteries. *ACS Appl. Mater. Interfaces* **2018**, *10*, 7946–7954. [CrossRef]

22. Liang, J.; Li, X.; Zhu, Y.; Guo, C.; Qian, Y. Hydrothermal synthesis of nano-silicon from a silica sol and its use in lithium ion batteries. *Nano Res.* **2015**, *8*, 1497–1504. [CrossRef]

23. Zong, L.; Jin, Y.; Liu, C.; Zhu, B.; Hu, X.; Lu, Z.; Zhu, J. Precise Perforation and Scalable Production of Si Particles from Low-Grade Sources for High-Performance Lithium Ion Battery Anodes. *Nano Lett.* **2016**, *16*, 7210–7215. [CrossRef]

24. Huang, Y.; Hou, X.; Fan, X.; Ma, S.; Hu, S.; Lam, K.-h. Advanced Li-Rich Cathode Collaborated with Graphite/Silicon Anode for High Performance Li-Ion Batteries in Half and Full Cells. *Electrochim. Acta* **2015**, *182*, 1175–1187. [CrossRef]

25. Tang, B.; He, S.; Deng, Y.; Shan, Y.; Qin, H.; Noor, H.; Hou, X. Advanced binder with ultralow-content for high performance silicon anode. *J. Power Sources* **2023**, *556*, 232237. [CrossRef]

26. Liang, J.; Wei, D.; Lin, N.; Zhu, Y.; Li, X.; Zhang, J.; Fan, L.; Qian, Y. Low temperature chemical reduction of fusional sodium metasilicate nonahydrate into a honeycomb porous silicon nanostructure. *Chem. Commun.* **2014**, *50*, 6856–6859. [CrossRef]

27. Zhuang, J.C.; Xu, X.; Peleckis, G.; Hao, W.C.; Dou, S.X.; Du, Y. Silicene: A Promising Anode for Lithium-Ion Batteries. *Adv. Mater.* **2017**, *29*, 1606716. [CrossRef]

28. Hong, J.E.; Lee, Y.; Mo, S.I.; Jeong, H.S.; An, J.H.; Song, H.E.; Oh, J.; Bang, J.; Oh, J.H.; Kim, K.H. Fully Bottom-Up Waste-Free Growth of Ultrathin Silicon Wafer via Self-Releasing Seed Layer. *Adv. Mater.* **2021**, *33*, e2103708. [CrossRef]

29. Chen, X.Q.; Zhang, Y.M.; Lin, H.B.; Xia, P.; Cai, X.; Li, X.G.; Li, X.P.; Li, W.S. Porous ZnMn$_2$O$_4$ nanospheres: Facile synthesis through microemulsion method and excellent performance as anode of lithium ion battery. *J. Power Sources* **2016**, *312*, 137–145. [CrossRef]

30. Liu, N.; Wu, H.; McDowell, M.T.; Yao, Y.; Wang, C.; Cui, Y. A yolk-shell design for stabilized and scalable li-ion battery alloy anodes. *Nano Lett.* **2012**, *12*, 3315–3321. [CrossRef]

31. Liang, C.; Sui, X.Y.; Wang, A.C.; Chang, J.Q.; Wang, W.B.; Chen, Z.X.; Jiang, W.Y.; Ma, Y.H.; Zhang, J.Q.; Liu, X.F.; et al. Controlled Production of MoS$_2$ Full-Scale Nanosheets and Their Strong Size Effects. *Adv. Mater. Interfaces* **2020**, *7*, 2001130. [CrossRef]

32. Nzabahimana, J.; Liu, Z.; Guo, S.; Wang, L.; Hu, X. Top-Down Synthesis of Silicon/Carbon Composite Anode Materials for Lithium-Ion Batteries: Mechanical Milling and Etching. *ChemSusChem* **2020**, *13*, 1923–1946. [CrossRef]

33. Lee, B.S. A Review of Recent Advancements in Electrospun Anode Materials to Improve Rechargeable Lithium Battery Performance. *Polymers* **2020**, *12*, 2035. [CrossRef]

34. Huang, A.; Ma, Y.; Peng, J.; Li, L.; Chou, S.-l.; Ramakrishna, S.; Peng, S. Tailoring the structure of silicon-based materials for lithium-ion batteries via electrospinning technology. *eScience* **2021**, *1*, 141–162. [CrossRef]

35. Lee, J.H.; Park, H.K.; Kim, J.H.; Jang, J.H.; Hong, S.K.; Oh, I.H. Constitutive behavior and microstructural evolution in Ti-Al-Si ternary alloys processed by mechanical milling and spark plasma sintering. *J. Mater. Res. Technol.* **2020**, *9*, 2247–2258. [CrossRef]

36. Li, H.; Li, H.; Lai, Y.; Yang, Z.; Yang, Q.; Liu, Y.; Zheng, Z.; Liu, Y.; Sun, Y.; Zhong, B.; et al. Revisiting the Preparation Progress of Nano-Structured Si Anodes toward Industrial Application from the Perspective of Cost and Scalability. *Adv. Energy Mater.* **2022**, *12*, 2102181. [CrossRef]

37. Kumar, M.; Xiong, X.; Wan, Z.; Sun, Y.; Tsang, D.C.W.; Gupta, J.; Gao, B.; Cao, X.; Tang, J.; Ok, Y.S. Ball milling as a mechanochemical technology for fabrication of novel biochar nanomaterials. *Bioresour. Technol.* **2020**, *312*, 123613. [CrossRef]

38. Qi, G.D.; Pan, Z.F.; Zhang, X.Y.; Miao, X.D.; Xiang, W.; Gao, B. Effect of ball milling with hydrogen peroxide or ammonia hydroxide on sorption performance of volatile organic compounds by biochar from different pyrolysis temperatures. *Chem. Eng. J.* **2022**, *450*, 138027. [CrossRef]

39. Jicsinszky, L.; Caporaso, M.; Tuza, K.; Martina, K.; Calcio Gaudino, E.; Cravotto, G. Nucleophilic Substitutions of 6I-O-Monotosyl-β-cyclodextrin in a Planetary Ball Mill. *ACS Sustain. Chem. Eng.* **2016**, *4*, 919–929. [CrossRef]

40. El-Sayed, T.H.; Aboelnaga, A.; El-Atawy, M.A.; Hagar, M. Ball Milling Promoted N-Heterocycles Synthesis. *Molecules* **2018**, *23*, 1348. [CrossRef]

41. Kubota, K.; Pang, Y.D.; Miura, A.; Ito, H. Redox reactions of small organic molecules using ball milling and piezoelectric materials. *Science* **2019**, *366*, 1500–1504. [CrossRef]

42. Nicholson, W.I.; Barreteau, F.; Leitch, J.A.; Payne, R.; Priestley, I.; Godineau, E.; Battilocchio, C.; Browne, D.L. Direct Amidation of Esters by Ball Milling. *Angew. Chem. Int. Ed.* **2021**, *60*, 21868–21874. [CrossRef]

43. De Bondt, Y.; Liberloo, I.; Roye, C.; Windhab, E.J.; Lamothe, L.; King, R.; Courtin, C.M. The Effect of Wet Milling and Cryogenic Milling on the Structure and Physicochemical Properties of Wheat Bran. *Foods* **2020**, *9*, 1755. [CrossRef]

44. El-Eskandarany, M.S. *Mechanical Alloying: Nanotechnology, Materials Science and Powder Metallurgy*; Elsevier: Amsterdam, The Netherlands, 2015.

45. Austin, L.G.; Bagga, P. An analysis of fine dry grinding in ball mills. *Powder Technol.* **1981**, *28*, 83–90. [CrossRef]

46. Salur, E.; Aslan, A.; Kuntoğlu, M.; Acarer, M.J.A.P.T. Effect of ball milling time on the structural characteristics and mechanical properties of nano-sized Y_2O_3 particle reinforced aluminum matrix composites produced by powder metallurgy route. *Adv. Powder Technol.* **2021**, *32*, 3826–3844. [CrossRef]

47. Zhuman, B.; Saepurahman; Anis, S.F.; Hashaikeh, R. Obtaining high crystalline ball milled H-Y zeolite particles with carbon nanostructures as a damping material. *Microporous Mesoporous Mater.* **2019**, *273*, 19–25. [CrossRef]

48. Shashanka, R.; Chaira, D. *Ball Milled Nano-Structured Stainless Steel Powders: Fabrication and Characterization*; Educreation Publishing: New Delhi, India, 2017.

49. Dou, F.; Shi, L.; Chen, G.; Zhang, D. Silicon/Carbon Composite Anode Materials for Lithium-Ion Batteries. *Electrochem. Energy Rev.* **2019**, *2*, 149–198. [CrossRef]

50. Cetinkaya, T.; Cevher, O.; Tocoglu, U.; Guler, M.O.; Akbulut, H. Electrochemical Characterization of the Powder Silicon Anodes Reinforced with Graphite Using Planetary Ball Milling. *Acta. Phys. Pol. A* **2013**, *123*, 393–395. [CrossRef]

51. Gauthier, M.; Mazouzi, D.; Reyter, D.; Lestriez, B.; Moreau, P.; Guyomard, D.; Roue, L. A low-cost and high performance ball-milled Si-based negative electrode for high-energy Li-ion batteries. *Energy Env. Sci.* **2013**, *6*, 2145–2155. [CrossRef]

52. Chen, M.; Duan, P.; Zhong, Y.; Wu, Z.; Zhang, Z.; Wang, Y.; Guo, X.; Wang, X. Constructing a Sheet-Stacked Si/C Composite by Recycling Photovoltaic Si Waste for Li-Ion Batteries. *Ind. Eng. Chem. Res.* **2022**, *61*, 2809–2816. [CrossRef]

53. Zhang, Y.; Ma, H.; Yu, C.; Feng, X. Si nanoplates prepared by ball milling photovoltaic silicon sawdust waste as lithium-ion batteries anode material. *Mater. Lett.* **2023**, *331*, 133469. [CrossRef]

54. Koraag, P.Y.E.; Firdaus, A.M.; Hawari, N.H.; Refino, A.D.; Dempwolf, W.; Iskandar, F.; Peiner, E.; Wasisto, H.S.; Sumboja, A. Covalently Bonded Ball-Milled Silicon/CNT Nanocomposite as Lithium-Ion Battery Anode Material. *Batteries* **2022**, *8*, 165. [CrossRef]

55. Ma, D.; Cao, Z.; Hu, A. Si-Based Anode Materials for Li-Ion Batteries: A Mini Review. *Nanomicro. Lett.* **2014**, *6*, 347–358. [CrossRef]

56. Kim, D.-W.; Kil, H.-S.; Kim, J.; Mochida, I.; Nakabayashi, K.; Rhee, C.K.; Miyawaki, J.; Yoon, S.-H. Highly graphitized carbon from non-graphitizable raw material and its formation mechanism based on domain theory. *Carbon* **2017**, *121*, 301–308. [CrossRef]

57. Wang, C.S.; Wu, G.T.; Zhang, X.B.; Qi, Z.F.; Li, W.Z. Lithium insertion in carbon-silicon composite materials produced by mechanical milling. *J. Electrochem. Soc.* **1998**, *145*, 2751–2758. [CrossRef]

58. Wilson, A.; Dahn, J. Lithium insertion in carbons containing nanodispersed silicon. *J. Electrochem. Soc.* **1995**, *142*, 326. [CrossRef]

59. Cabello, M.; Gucciardi, E.; Herran, A.; Carriazo, D.; Villaverde, A.; Rojo, T. Towards a High-Power Si@graphite Anode for Lithium Ion Batteries through a Wet Ball Milling Process. *Molecules* **2020**, *25*, 2494. [CrossRef]

60. Yoshio, M.; Tsumura, T.; Dimov, N. Silicon/graphite composites as an anode material for lithium ion batteries. *J. Power Sources* **2006**, *163*, 215–218. [CrossRef]

61. Cetinkaya, T.; Guler, M.O.; Akbulut, H. Enhancing electrochemical performance of silicon anodes by dispersing MWCNTs using planetary ball milling. *Microelectron. Eng.* **2013**, *108*, 169–176. [CrossRef]

62. Cameán, I.; Garcia, A.B. Graphite materials prepared by HTT of unburned carbon from coal combustion fly ashes: Performance as anodes in lithium-ion batteries. *J. Power Sources* **2011**, *196*, 4816–4820. [CrossRef]

63. Zhang, Y.; Cheng, Y.Q.; Song, J.H.; Zhang, Y.J.; Shi, Q.; Wang, J.X.; Tian, F.H.; Yuan, S.; Su, Z.; Zhou, C.; et al. Functionalization-assistant ball milling towards Si/graphene anodes in high performance Li-ion batteries. *Carbon* **2021**, *181*, 300–309. [CrossRef]

64. Shi, W.Y.; Wu, H.B.; Baucom, J.; Li, X.Y.; Ma, S.X.; Chen, G.; Lu, Y.F. Covalently Bonded Si-Polymer Nanocomposites Enabled by Mechanochemical Synthesis as Durable Anode Materials. *ACS Appl. Mater. Interfaces* **2020**, *12*, 39127–39134. [CrossRef]

65. Dong, Z.; Gu, H.; Du, W.; Feng, Z.; Zhang, C.; Jiang, Y.; Zhu, T.; Chen, G.; Chen, J.; Liu, Y.; et al. Si/Ti$_3$SiC$_2$ composite anode with enhanced elastic modulus and high electronic conductivity for lithium-ion batteries. *J. Power Sources* **2019**, *431*, 55–62. [CrossRef]

66. Cao, Y.; Scott, B.; Dunlap, R.A.; Wang, J.; Obrovac, M.N. An Investigation of the Fe-Mn-Si System for Li-Ion Battery Negative Electrodes. *J. Electrochem. Soc.* **2019**, *166*, A21–A26. [CrossRef]

67. Liu, X.; Dai, Y.; Xie, J.Y.; Zhao, H.L.; Lv, P.P.; Wang, K.; Swierczek, K. Improvement of silicon-based electrode for Li-ion batteries by formation of Si-TiB$_2$-C nanocomposites. *Solid State Ion.* **2015**, *281*, 60–67. [CrossRef]

68. Pan, W.; Cai, X.; Yang, C.; Zhou, L. Amorphous Si/TiC/Graphite Composite Fabricated by High-Energy Ball-Milling as an Anode for Lithium-Ion Batteries. *J. Electron. Mater.* **2021**, *50*, 2584–2593. [CrossRef]

69. Sbrascini, L.; Staffolani, A.; Bottoni, L.; Darjazi, H.; Minnetti, L.; Minicucci, M.; Nobili, F. Structural and Interfacial Characterization of a Sustainable Si/Hard Carbon Composite Anode for Lithium-Ion Batteries. *ACS Appl. Mater. Interfaces* **2022**, *14*, 33257–33273. [CrossRef]

70. Liu, S.; Tao, W.; Yu, Y.; Fakudze, S.; Wang, C.; Wang, J.; Han, J.; Chen, J. Ball milling synthesis of robust sandwich-structured C/Si@SnO$_2$ anode with porous silicon buffer layer for fast charging lithium-ion battery. *Colloids Surf. A Physicochem. Eng. Asp.* **2022**, *654*, 130088. [CrossRef]

71. He, Y.; Ye, Z.; Chamas, M.; Sougrati, M.T.; Lippens, P.-E. Si/Cu-Zn(ox)/C composite as anode material for Li-ion batteries. *Solid State Ion.* **2021**, *372*, 115774. [CrossRef]

72. Wang, J.; Zhang, X.; Wang, R.; Tan, G.; Su, Y.; Wu, F. Preparation and electrochemical performance of porous Si/SiO$_x$/G composite anode for lithium ion batteries. *IOP Conf. Ser. Mater. Sci. Eng.* **2020**, *735*, 012015. [CrossRef]

73. Zhao, F.; Zhao, M.; Dong, Y.; Ma, L.; Zhang, Y.; Niu, S.; Wei, L. Facile preparation of micron-sized silicon-graphite-carbon composite as anode material for high-performance lithium-ion batteries. *Powder Technol.* **2022**, *404*, 117455. [CrossRef]

74. Nguyen, Q.H.; Kim, I.T.; Hur, J. Core-shell Si@c-PAN particles deposited on graphite as promising anode for lithium-ion batteries. *Electrochim. Acta* **2019**, *297*, 355–364. [CrossRef]

75. Nulu, A.; Nulu, V.; Sohn, K.Y. Silicon and porous MWCNT composite as high capacity anode for lithium-ion batteries. *Korean J. Chem. Eng.* **2020**, *37*, 1795–1802. [CrossRef]

76. Zhang, P.; Gao, Y.; Ru, Q.; Yan, H.; Chen, F.; Ling, F.C.-C. Scalable preparation of porous nano-silicon/TiN@carbon anode for lithium-ion batteries. *Appl. Surf. Sci.* **2019**, *498*, 143829. [CrossRef]

77. Chung, W.-Y.; Brahma, S.; Hou, S.-C.; Chang, C.-C.; Huang, J.-L. Petroleum waste hydrocarbon resin as a carbon source modified on a Si composite as a superior anode material in lithium ion batteries. *Mater. Chem. Phys.* **2021**, *259*, 124011. [CrossRef]

78. Miao, R.; Zhu, J.; Kang, S.; Yang, J.; Wang, J.; Fu, J.; Li, M.; Shi, C. In-situ mechanochemical synthesis of sub-micro Si/Sn@SiO$_x$-C composite as high-rate anode material for lithium-ion batteries. *Electrochim. Acta* **2021**, *384*, 138413. [CrossRef]

79. Wu, Y.S.; Yang, C.C.; Wu, S.H.; Wu, Z.H.; Wei, C.N.; Yang, M.Y.; Lue, S.J. Preparation of ternary hierarchical silicon/reduced graphene oxide/carbon composites as anodes for lithium–ion batteries. *J. Alloys Compd.* **2019**, *793*, 433–445. [CrossRef]

80. Du, Y.; Yang, Z.; Yang, Y.; Yang, Y.; Jin, H.; Hou, G.; Yuan, F. Mussel-pearl-inspired design of Si/C composite for ultrastable lithium storage anodes. *J. Alloys Compd.* **2021**, *872*, 159717. [CrossRef]

81. Wang, X.; Wen, K.; Chen, T.; Chen, S.; Zhang, S. Supercritical fluid-assisted preparation of Si/CNTs@FG composites with hierarchical conductive networks as a high-performance anode material. *Appl. Surf. Sci.* **2020**, *522*, 146507. [CrossRef]

82. Dong, H.; Fu, X.; Wang, J.; Wang, P.; Ding, H.; Song, R.; Wang, S.; Li, R.; Li, S. In-situ construction of porous Si@C composites with LiCl template to provide silicon anode expansion buffer. *Carbon* **2021**, *173*, 687–695. [CrossRef]

83. Li, J.Y.; Li, G.; Zhang, J.; Yin, Y.X.; Yue, F.S.; Xu, Q.; Guo, Y.G. Rational Design of Robust Si/C Microspheres for High-Tap-Density Anode Materials. *ACS Appl. Mater. Interfaces* **2019**, *11*, 4057–4064. [CrossRef] [PubMed]

84. Zhang, Z.; Sun, S.; Zhang, W.; Xu, J.; Wang, X.; Fang, C.; Li, Q.; Han, J. Internally inflated core-buffer-shell structural Si/EG/C composites as high-performance anodes for lithium-ion batteries. *Sci. China Mater.* **2022**, *65*, 2949–2957. [CrossRef]

85. Miyachi, M.; Yamamoto, H.; Kawai, H.; Ohta, T.; Shirakata, M. Analysis of SiO Anodes for Lithium-Ion Batteries. *J. Electrochem. Soc.* **2005**, *152*, A2089. [CrossRef]

86. Chen, T.; Wu, J.; Zhang, Q.; Su, X. Recent advancement of SiO$_x$ based anodes for lithium-ion batteries. *J. Power Sources* **2017**, *363*, 126–144. [CrossRef]

87. Ouyang, P.H.; Jin, C.X.; Xu, G.J.; Yang, X.X.; Kong, K.J.; Liu, B.B.; Dan, J.L.; Chen, J.; Yue, Z.H.; Li, X.M.; et al. Lithium ion batteries with enhanced electrochemical performance by using carbon-coated SiO$_x$/Ag composites as anode material. *Ceram. Int.* **2021**, *47*, 1086–1094. [CrossRef]

88. Yuan, T.; Tang, R.; Xiao, F.; Zuo, S.; Wang, Y.; Liu, J. Modifying SiO as a ternary composite anode material((SiO$_x$/G/SnO$_2$)@C) for Lithium battery with high Li-ion diffusion and lower volume expansion. *Electrochim. Acta* **2023**, *439*, 141655. [CrossRef]

89. Wang, P.; Hou, S.; Pang, F.; Liu, M.; Li, Y.X.; Liu, T.Z.; Luo, Y.Z.; Fan, Y.M.; Zhao, L.Z. SiO$_x$/C-Decorated CoO Nanosheets as a Long-life Anode for Lithium-Ion Batteries. *Chemelectrochem* **2019**, *6*, 1574–1581. [CrossRef]

90. Zhang, K.; Du, W.; Qian, Z.; Lin, L.; Gu, X.; Yang, J.; Qian, Y. SiO$_x$ embedded in N-doped carbon nanoslices: A scalable synthesis of high-performance anode material for lithium-ion batteries. *Carbon* **2021**, *178*, 202–210. [CrossRef]

91. Si, Q.; Hanai, K.; Ichikawa, T.; Phillipps, M.B.; Hirano, A.; Imanishi, N.; Yamamoto, O.; Takeda, Y. Improvement of cyclic behavior of a ball-milled SiO and carbon nanofiber composite anode for lithium-ion batteries. *J. Power Sources* **2011**, *196*, 9774–9779. [CrossRef]

92. Zheng, C.-H.; Zhang, G.-P.; Wang, S.-S.; Mao, A.-Q.; Fang, D.-L. Efficient transformation of rice husk to a high-performance Si@SiO$_2$@C anode material by a mechanical milling and molten salt coactivated magnesiothermic reduction. *J. Alloy. Compd.* **2021**, *875*, 159974. [CrossRef]

93. Yang, M.; Jin, L.; He, M.; Yi, Z.; Duan, T.; Yao, W. SiO$_x$@C composites obtained by facile synthesis as anodes for lithium- and potassium-ion batteries with excellent electrochemical performance. *Appl. Surf. Sci.* **2021**, *542*, 148712. [CrossRef]

94. Xu, D.; Chen, W.; Luo, Y.; Wei, H.; Yang, C.; Cai, X.; Fang, Y.; Yu, X. Amorphous TiO$_2$ layer on silicon monoxide nanoparticles as stable and scalable core-shell anode materials for high performance lithium ion batteries. *Appl. Surf. Sci.* **2019**, *479*, 980–988. [CrossRef]

95. Hwang, J.; Kim, K.; Jung, W.-S.; Choi, H.; Kim, J.-H. Facile and scalable synthesis of SiO$_x$ materials for Li-ion negative electrodes. *J. Power Sources* **2019**, *436*, 226883. [CrossRef]

96. Park, D.; Kim, H.-S.; Seo, H.; Kim, K.; Kim, J.-H. Porous SiO composite tailored by scalable mechanochemical oxidation of Si for Li-ion anodes. *Electrochim. Acta* **2020**, *357*, 136862. [CrossRef]

97. Feng, Y.; Liu, X.; Liu, L.; Zhang, Z.; Teng, Y.; Yu, D.; Sui, J.; Wang, X.J.C. SiO$_2$/C Composite Derived from Rice Husks with Enhanced Capacity as Anodes for Lithium-Ion Batteries. *ChemistrySelect* **2018**, *3*, 10338–10344. [CrossRef]

98. Park, B.H.; Haghighat-Shishavan, S.; Nazarian-Samani, M.; Kim, K.-B. High-performance silicon diphosphide/nanocarbon composite anode for Li-ion batteries: Role of chemical bonding and interfaces in the establishment of cycling stability. *J. Power Sources* **2019**, *434*, 226759. [CrossRef]

99. Li, W.; Ma, Q.; Shen, P.; Zhou, Y.; Soule, L.; Li, Y.; Wu, Y.; Zhang, H.; Liu, M. Yolk-shell structured CuSi$_2$P$_3$@Graphene nanocomposite anode for long-life and high-rate lithium-ion batteries. *Nano Energy* **2021**, *80*, 105506. [CrossRef]

100. Li, W.W.; Liao, J.; Li, X.W.; Zhang, L.; Zhao, B.T.; Chen, Y.; Zhou, Y.C.; Cuo, Z.P.; Liu, M.L. Zn(Cu)Si$_2$+xP$_3$ Solid Solution Anodes for High-Performance Li-Ion Batteries with Tunable Working Potentials. *Adv. Funct. Mater.* **2019**, *29*, 1903638. [CrossRef]

101. Liu, X.; Zhao, Y.; Li, Y.; Li, W. AlSixP: A new family of ternary Si-based anodes for Li-ion batteries with superior Li-storage properties. *Ceram. Int.* **2023**, *49*, 1535–1539. [CrossRef]

102. Chen, D.; Yi, R.; Chen, S.; Xu, T.; Gordin, M.L.; Wang, D. Facile synthesis of graphene–silicon nanocomposites with an advanced binder for high-performance lithium-ion battery anodes. *Solid State Ion.* **2014**, *254*, 65–71. [CrossRef]

103. Zhang, Q.L.; Xi, B.J.; Xiong, S.L.; Qian, Y.T. Carbon coated SiO nanoparticles embedded in hierarchical porous N-doped carbon nanosheets for enhanced lithium storage. *Inorg.Chem. Front.* **2021**, *8*, 4282–4290. [CrossRef]

104. Zhang, B.; Wang, H.; Liu, C.; Li, D.; Kim, H.-K.; Harris, C.; Lao, C.-Y.; Abdelkader, A.; Xi, K. Facile mechanochemical synthesis of non-stoichiometric silica-carbon composite for enhanced lithium storage properties. *J. Alloys Compd.* **2019**, *801*, 658–665. [CrossRef]

105. Ruttert, M.; Siozios, V.; Winter, M.; Placke, T. Mechanochemical Synthesis of Fe–Si-Based Anode Materials for High-Energy Lithium Ion Full-Cells. *ACS Appl. Energy Mater.* **2019**, *3*, 743–758. [CrossRef]

106. Wu, Z.-Y.; Wu, C.-Y.; Duh, J.-G. Facile synthesis of boron-doped graphene-silicon conductive network composite from recycling silicon for Lithium-ion batteries anodes materials. *Mater. Lett.* **2021**, *296*, 129875. [CrossRef]